Increased susceptibility to spontaneous lung cancer in mice lacking LIM-domain only 7

Miki Tanaka-Okamoto,[1] Keiko Hori,[1] Hiroyoshi Ishizaki,[1,2] Akihiro Hosoi,[1] Yu Itoh,[1] Min Wei,[3] Hideki Wanibuchi,[3] Akira Mizoguchi,[4] Hiroyuki Nakamura[5] and Jun Miyoshi[1,6]

[1]Department of Molecular Biology, Osaka Medical Center for Cancer and Cardiovascular Diseases, Osaka; [2]KAN Research Institute, Kobe; [3]Department of Pathology, Osaka City University Medical School, Osaka; [4]Department of Anatomy, Mie University Medical School, Tsu; [5]Department of Biochemistry, Osaka Medical Center for Cancer and Cardiovascular Diseases, Osaka, Japan

(Received October 3, 2008/Revised December 4, 2008; December 12, 2008/Accepted December 21, 2008/Online publication February 2, 2009)

LIM-domain only (LMO) 7 is a multifunctional protein that is predicted to regulate the actin cytoskeleton, assembly of adherens junctions in epithelial cells, and gene expression. LMO7 was highly expressed in the mouse lung and predominantly localized to the apical membrane domain of bronchiolar epithelial cells. Although mice lacking LMO7 were viable and fertile in specific pathogen-free conditions, they developed protruding epithelial lesions in the terminal and respiratory bronchioles and alveolar ducts at 14–15 weeks of age. Furthermore, they tended to develop spontaneous adenocarcinoma in the lung at over 90 weeks of age. The cumulative incidence ratios of lung cancer were 22% in *LMO7*$^{-/-}$ mice and 13% in *LMO7*$^{+/-}$ mice whereas no primary lung cancer was observed in wild-type mice. *Ex vivo* analyses of the cancer cells showed numerical chromosome abnormalities and tumorigenicity in nude mice. These results suggest that LMO7 can act as a tumor suppressor whose deficiency confers a genetic predisposition to naturally occurring lung cancer. (*Cancer Sci* 2009; 100: 608–616)

Adherens junctions are specialized cell–cell attachments composed of transmembrane proteins, such as E-cadherin and nectins, and cytoplasmic proteins, such as catenins and afadin, which anchor to the actin cytoskeleton.[1] AJ have prototypic roles in stabilizing the epithelium, establishing apical–basal polarity of epithelial cells and facilitating cell–cell communication that regulates cell proliferation and movement.[2–4] Loss of AJ, as well as aberrant signaling involving the Wnt pathway, could contribute to carcinogenesis and metastasis by causing cell depolarization, loss of contact-dependent inhibition of proliferation, and increased motility and invasiveness.[5–8] Cancer cells frequently undergo EMT with the induction of transcriptional repressor proteins such as the snail transcription factor, slug, and Twist, which downregulate E-cadherin gene expression. EMT seems to be a basic mechanism that mediates disruption of epithelial polarity and disintegration of cancer cell nests.[9] Because most human cancers are of epithelial origin, disruption of AJ is one of the hallmarks of cancer cells undergoing malignant transformation.

LIM-domain only 7 is a member of a protein family composed of nine proteins containing both PDZ and LIM domains that function as protein–protein recognition modules.[10,11] The PDZ and LIM family proteins are generally thought to be involved in forming the Z-band of muscle through their PDZ domains that bind to α-actinin or β-tropomyosin and are directly or indirectly linked to the actin cytoskeleton.[12–19] In contrast, a yeast two-hybrid study has shown that LMO7 also binds afadin, the adaptor protein of nectins, at AJ through the LIM domain.[16] Although these observations suggest a role for LMO7 in the formation and maintenance of epithelial architecture via remodeling of the actin cytoskeleton, it is not well understood how LMO7 exhibits its physiological functions at AJ.

On the other hand, evidence is accumulating that LMO7 is implicated in cancer-related pathological conditions. First, we previously isolated an LMO7 splice variant truncated in the C-terminal region, originally described as the *#16* gene product, by subtraction and differential hybridization from Yoshida hepatoma AH130W1 cells treated with TGF-β.[20] TGF-β induced alternative splicing of the *LMO7* gene, as well as the ability of AH130W1 cells to migrate during an *in vitro* invasion assay.[21,22] Second, elevated levels of LMO7 expression, also known as PCD1, have been reported in pancreatic and colon cancers.[23–25] Third, LMO7 is actually involved in gene expression by acting as a nucleocytoplasmic shuttling protein that regulates the transcription of emerin and muscle-relevant genes.[26] Finally, the *LMO7* gene is located on human chromosome 13q22, which is implicated in hereditary cancer of the mammary glands.[27,28] LMO7 may be the responsible tumor suppressor, although it is controversial whether mutations involving LMO7 or those involving flanking genes actually cause hereditary mammary cancer.[27–29] Therefore, it is intriguing to examine whether LMO7 is implicated in the initiation, promotion, or progression of cancer in animal models.

Here we report phenotypes of *LMO7*-deficient mice in a long-term analysis. The mice developed irregular and protruding epithelial lesions in the terminal and respiratory bronchioles at younger ages, and they tended to develop naturally occurring lung cancer at older ages. Histologically, these tumors were diagnosed as adenocarcinomas and the lung cancer cells were further characterized *ex vivo*. We propose that *LMO7* may act as a tumor suppressor in the sense that its deficiency at least provides mice with a genetic predisposition to spontaneous lung cancer.

Materials and Methods

Antibodies. Recombinant proteins containing 393–670 amino acid residues of rat P100 #16/LMO7 (GeneBank accession number AY609384) and other regions were constructed as fusion proteins with glutathione S transferase using the pGEX plasmid vector (GE Healthcare UK, Buckinghamshire, UK) and used as an immunogen (Fig. 1a). Rabbit polyclonal antibodies #3528 and #863, as well as monoclonal antibodies Mab15A and Mab12A, were raised against the LMO7–glutathione S transferase fusion proteins. Polyclonal antibodies were affinity purified. Rabbit polyclonal antibodies NO2 and CO5 were kindly provided by Dr Takai at Kobe University (Kobe, Japan). All of the following

[6]To whom correspondence should be addressed. E-mail: miyosi-ju@mc.pref.osaka.jp
Abbreviations: AJ, adherens junction; EMT, epithelial–mesenchymal transition; LIM, Lin-11, Isl-1, and Mec-3; LMO, LIM-domain only; PCR, polymerase chain reaction; PDZ, PSD95, DlgA, and ZO-1; TGF, transforming growth factor; Uchl3, ubiquitin C-terminal hydrolase L3; WT, wild type.

doi: 10.1111/j.1349-7006.2009.01091.x

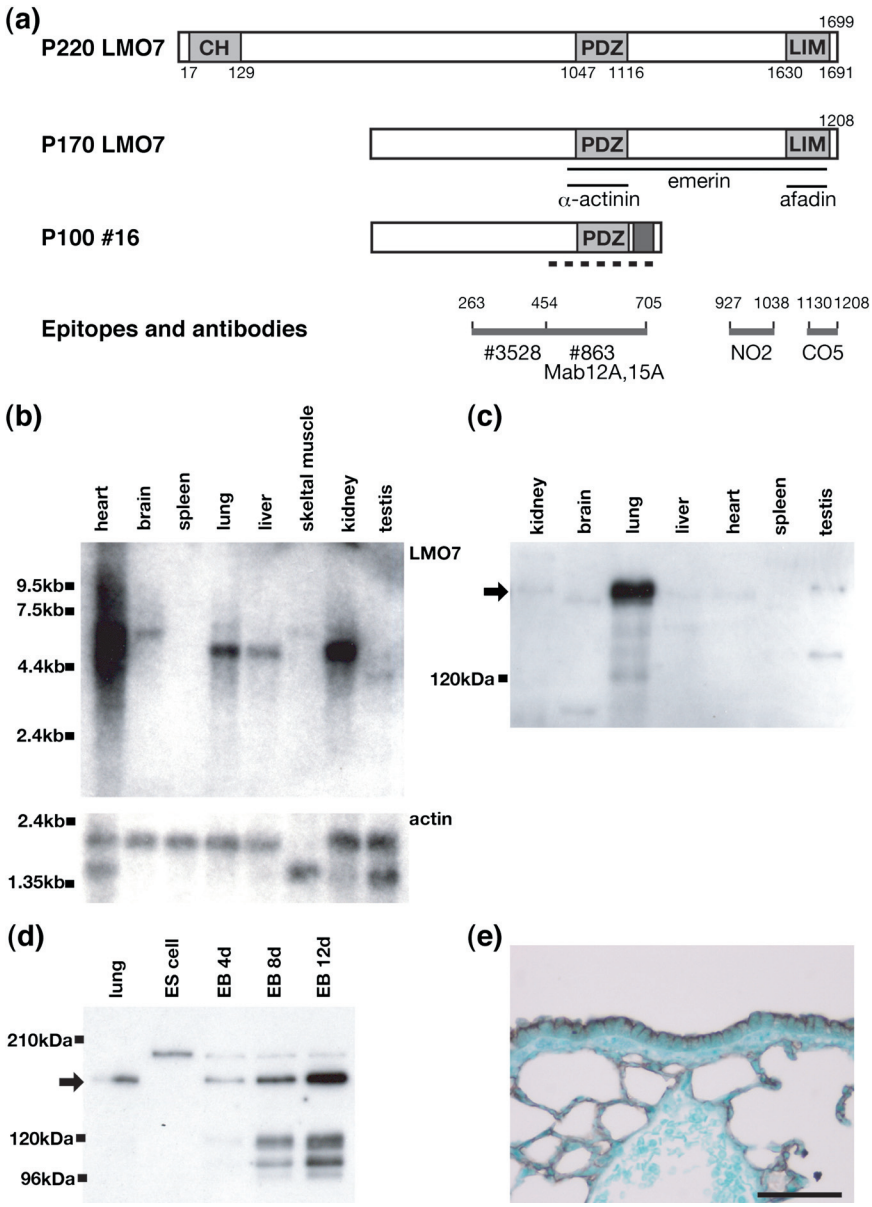

Fig. 1. Molecular structure and expression profile of LIM-domain only (LMO) 7. (a) Schematic structures of three isoforms of LMO7 and antibodies with relevant epitopes. LMO7 contains one PSD95, DlgA, and ZO-1 (PDZ) domain and one LIM domain. The binding sites with α-actinin, afadin, and emerin, as well as the regions for antigens to produce anti-LMO7 antibodies, are shown by solid lines. (b) Northen blot analysis of LMO7. LMO7 mRNA was ubiquitously expressed in several mouse tissues including the heart, kidney, lung, liver, and brain. (c) Expression profiles of LMO7 proteins in mouse tissues. P170 LMO7 indicated by the arrow was predominantly detected in the mouse lung by immunoprecipitation and immunoblot analyses using polyclonal antibody #863. Experiments were repeated using different antibodies and representative cases are shown. (d) Expression of LMO7 during embryoid body formation. As the embryonic stem cells differentiated, the predominant LMO7 protein shifted from 200 to 170 kDa. Total cell extracts were immunoprecipitated with the anti-LMO7 antibody #863, and then the immunoprecipitates were resolved by sodium dodecylsulfate–polyacrylamide gel electrophoresis and immunoblotted with the same antibody. (e) Immunohistochemistry of the LMO7 protein in the mouse lung section using an anti-LMO7 antibody raised against the PDZ domain. The sections were counterstained with methyl green. LMO7 was detected at the apical surface in epithelial cells of the bronchioles and alveolar cells. Scale bar = 50 μm (upper panels), scale bar = 10 μm (lower panels). EB, embrioid body; ES cells, embryonic stem cells.

antibodies were purchased from commercial sources: anti-afadin and anti-nectin-3 antibodies (ABcam, Cambridge, UK), anti-ezrin antibody (Invitrogen, Carlsbad, CA, USA, and Cell Signaling, Beverly, MA, USA), anti-nectin-2 antibody (Hycult, Bangkok, Thailand), anti-E-cadherin antibody (R&D Systems, Minneapolis, MN, USA), anti-actin (C4) antibody (Millipore Corporation, Billerica, MA, USA), anti-β-catenin antibody (BD Biosciences, San Jose, CA, USA), anti-α-actinin antibody (Millipore), anti-Ki67 antibody (Novocastra Laboratories, Newcastle, UK), anti-keratin antibody (LSL, Tokyo, Japan), and rhodamine–phalloidin and Alexa Fluor-labeled secondary antibodies (Invitrogen).

Generation of mice lacking *LMO7*. The targeting vector was constructed by inserting 5′- and 3′-homologous DNA fragments into an MC1-*neo*/MC1-DT-A cassette, designed to replace the 3′-half of exon 8 and following exon 9 encoding the PDZ domain of LMO7 for the neo-resistant gene cassette. Mouse 129/Sv-derived RW4 cells were electroporated with the linearized targeting vector to cause homologous recombination. DNA isolated from G418-resistant ES cells was screened by Southern hybridization. RW4 ES cells were cultured in Dulbecco's Modified Eagle's Medium as described previously.[30] Genotyping for mice was carried out by PCR using the following primers: 5′-GGGCGCCCGGTTCTTTTTGTC-3′ and 5′-GCCATGATGGATACTTTCTCG-3′ for the *neo* gene, and 5′-CAGCTGCAGGTAGATGATGAA-3′ and 5′-AACAACGATGACAAAACAACT-3′ for the mouse *LMO7* gene.

Immunoblotting analysis. Mouse tissues and embryoid bodies were solubilized with RIPA lysis buffer containing 50 mM Tris (pH 8.0), 150 mM NaCl, 1.0% Nonidet P-40, 0.5% deoxycholic acid, 0.1% sodium dodecylsulfate, 1 μg/mL aprotinin, 1 μg/mL leupeptin, and 20 μg/mL phenylmethylsulfonyl fluoride. The lysates were clarified by centrifugation at 10 000*g* for 10 min at 4°C, and the protein concentration of clarified extracts was determined using a protein assay kit (Bio-Rad Laboratories, Hercules, CA, USA). The adjusted samples were resolved in sodium dodecylsulfate–polyacrylamide gels and electrophoretically transferred to a polyvinylidene difluoride membrane, followed by incubation with primary antibodies. The blots were subsequently incubated with horseradish peroxidase-conjugated secondary

antibodies (Santa Cruz Biotechnologies, Santa Cruz, CA, USA) and with ECL western blotting detection reagents (GE Healthcare).

Immunofluorescence microscopy. Mouse lung sections were fixed in 20% formalin neutral buffer solution, embedded in paraffin, and sectioned at 3–4 μm thickness. After deparaffinization, sections were treated with heat and 10 mM sodium citrate buffer to unmask antigens. After blocking with 5% skim milk and 0.005% saponin in phophate-buffered saline, samples were incubated with primary antibodies and then with fluorescent or horseradish peroxidase-conjugated secondary antibodies. Fluorescence images were recorded on a charge-coupled device camera (Keyence, Osaka, Japan) and processed using Adobe Photoshop (Adobe System Incorporated, CA, USA).

Electron microscopy. Lung tissues were fixed with 2.5% glutaraldehyde and 2% paraformaldehyde in phosphate-buffered saline, followed by fixation with 1% OsO_4 in 0.1 M cacodylate-HCl, pH 7.4, for 1 h. The samples were dehydrated, embedded in Epon812, and examined using an electron microscope.

Northern blot analysis. The mouse mRNA blot (Clontech Laboratories, Palo Alto, CA, USA) was hybridized with the 1.7-kb N-terminal *Eco*RI fragment of the full-length P170 *LMO7* cDNA that was labeled with [α-^{32}P] dCTP as a probe.

Statistics. Statistical analysis was carried out using Fisher's direct method for intergroup comparisons. A *P*-value of <0.05 was accepted as being statistically significant.

Results

Structure and expression profiles of the LMO7 proteins. The mouse *LMO7* gene encodes several isoforms of LMO7.[16,20,31] Representative isoforms of LMO7 are shown schematically in Figure 1(a) with the organization of known domains and their binding proteins, as well as the regions used for raising antibodies. Besides the isoforms shown in Figure 1(a), we have actually obtained an LMO7 variant lacking the LIM domain from the mouse brain cDNA library (data not shown) whereas some isoforms containing the PDZ and LIM domains have been reported.[16] The largest isoform is a 220-kDa protein (P220 LMO7) encoded by the full-length *LMO7* cDNA. The PDZ and LIM domains interact with the actin-binding proteins α-actinin and afadin, respectively,[16] whereas the functional roles of the other domains are not fully understood.

To investigate the predominant LMO7 isoforms and their tissue-specific expression in adult mouse tissues, we carried out northern blot and immunoblot analyses (Fig. 1b,c). LMO7 transcripts were expressed ubiquitously in the lung, heart, brain, and kidney preparations, and several mRNA bands of different sizes were identified (Fig. 1b), basically consistent with the previous observations of PCD1 as analyzed by *in situ* hybridization.[23] In contrast, LMO7 proteins were expressed almost exclusively in the adult mouse lung (Fig. 1c), although they were expressed ubiquitously as examined by a long exposure of the same immunoblot. The predominant LMO7 isoform in the mouse lung was a 170-kDa protein (P170 LMO7) that was considerably smaller than P220 LMO7 deduced from the coding region of the full-length *LMO7* cDNA. Interestingly, P220 LMO7 was prominently expressed in embryonic stem cells, whereas it was replaced with P170 LMO7 during the developmental stages (Fig. 1d). Thus, P170 LMO7 appears to play predominant roles in the mouse lung after birth, although the physiological significance of the conversion from P220 LMO7 to P170 LMO7 remains unknown.

We next examined the cell type that expresses LMO7 in the lung. We raised several antibodies (Fig. 1a) and undertook immunostaining of mouse lung sections and found that LMO7 was expressed exclusively in epithelial cells of the terminal bronchioles, respiratory bronchioles, and alveolar ducts. Notably, LMO7 was localized to the luminal surface of epithelial cells (Fig. 1e). No significant immunostaining was observed after pre-

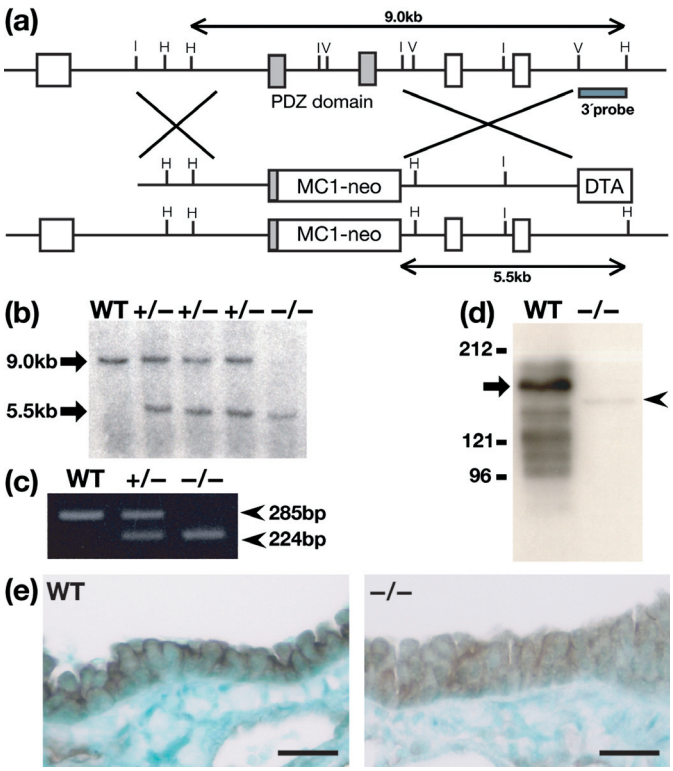

Fig. 2. Generation of LIM-domain only (*LMO*) 7$^{-/-}$ mice and immunohistochemistry of LMO7 in the bronchiolar epithelial cells. (a) Targeting strategy. The *LMO7* allele was to be disrupted and replaced by the neomycin-resistance gene by homologous recombination. (b) Genotyping of the mice was carried out by Southern hybridization using *Hind*III-digested genomic DNA and the 3′-probe. (c) Genotyping of the mice by polymerase chain reaction detecting the wild-type (WT) *LMO7*-specific band (285 bp) and the mutant-specific band for the *neo* gene (224 bp). (d) Western blot analysis of P170 LMO7 in the mouse lung. P170 LMO7 was absent in the *LMO7*$^{-/-}$ mice although proteins (arrowhead) smaller than P170 LMO7 (arrow), with decreased levels, were observed in the *LMO7*$^{-/-}$ mice. (e) Immunohistochemical staining of LMO7 in the lung from the WT and *LMO7*$^{-/-}$ mice. LMO7 was localized to the apical side of the epithelial cells in the WT but not in the *LMO7*$^{-/-}$ lung. Scale bar = 20 μm. DTA, Diphtheria Toxin A.

incubating the anti-LMO7 antibody with an LMO7–glutathione S-transferase fusion protein used as an immunogen (data not shown). LMO7 thus appears to play roles at the apical membrane domain or the apical junctions but not at the basolateral membrane domain of bronchiolar epithelial cells.

Generation of mice lacking LMO7. To gain more insight into the physiological roles of LMO7, we generated mice lacking LMO7. Because the mouse *LMO7* gene spans over 200 kb and is transcribed from several different promoters, it is difficult to disrupt the entire gene by a single step of conventional gene targeting. A gene deletion that covers 800 kb, including the *LMO7* and *Uchl3* genes, was generated by two independent events of homologous recombination using the Cre-loxP targeting strategy.[32] We then introduced a mutation that deleted the two exons of the *LMO7* gene encoding the PDZ domain into embryonic stem cells. Cells with targeted disruption of *LMO7* were screened by Southern hybridization, and genotyping of mice lacking *LMO7* was carried out by PCR analysis (Fig. 2a–c).

We confirmed the absence of P170 LMO7 in the lung of *LMO7*$^{-/-}$ mice (Fig. 2d). It is possible, however, that LMO7 proteins lacking the PDZ domain with internal deletion might be generated by in-frame alternative splicing between exons located 5′-upstream and 3′-downstream of the region replaced by the *neo*

doi: 10.1111/j.1349-7006.2009.01091.x

Table 1. Genotyping of LIM-domain only (LMO) 7-deficient mice obtained from heterozygous intercrossing

Genetic background	Genotype		
	Wild type	+/–	–/–
Mixed (129xB6xDBA2)	104 (27%)	182 (48%)	94 (25%)
B6:N4	17 (20%)	39 (46%)	29 (34%)
FVB:N4	17 (24%)	41 (57%)	14 (19%)

Table 2. Spontaneous lung cancer of LIM-domain only (LMO) 7-deficient mice

Genotype	No. lung tumor-bearing mice	
	F1 (129/DBA2/C57BL6)[‡]	C57BL6 (N4)[§]
Wild type	0/19	0/10
+/–	2/15 (13%)	1/16 (6%)
–/–	10/45 (22%)[†]	3/25 (12%)

[†]Fisher's direct method: homozygotes vs wild type; $P < 0.05$.
[‡]The genetic fraction of F_1: 129SV:C57BL/6 J:DBA2 = 50%:25%:25%.
[§]The genetic fraction of N4: 129SV:C57BL/6 J:DBA2 = 3.2%:95.2%:1.6%.

gene insertion. We actually detected additional bands that were smaller in size than P170 LMO7 in the immunoblots of *LMO7*$^{-/-}$ mouse lung but not in those of WT mouse lung (Fig. 2d). Compared with P170 LMO7, their expression levels were much lower and their precise sequences were unclear. As it was unknown whether the additional products have some dominant roles, we consider that the *LMO7*$^{-/-}$ mice should be bona fide null mutants for *LMO7* because they lack the exon encoding the PDZ domain, that plays critical roles in for protein–protein interactions between LMO7 and partner proteins.

We further characterized lung sections of the WT and *LMO7*$^{-/-}$ mice with anti-LMO7 antibodies raised against the region containing the PDZ domain, and then examined how the targeted disruption of *LMO7* affects the localization of LMO7 in epithelial cells. Lung sections of the *LMO7*$^{-/-}$ mice showed no signal at the apical membrane domain except non-specific signals in the entire cytoplasm of epithelial cells (Fig. 2e). These results suggest that the PDZ domain is essentially required for the localization of LMO7 at the apical membrane in lung epithelial cells.

Structural changes of epithelia in the lung of mice lacking LMO7. The genetic properties of mice used in the present study are summarized in Table 1. We compared the phenotypes of mice with several genetic backgrounds, ranging from F_1 hybrid mice (129:C57BL6:DBA2 = 2 : 1 : 1) to those backcrossed to C57BL6 or FVB mice for four generations. *LMO7*$^{-/-}$ mice were generated by intercrosses between *LMO7*$^{+/-}$ mice; litters of all of the genotypes were reproduced at the Mendelian ratio (Table 1). *LMO7*$^{-/-}$ mice were viable and fertile after birth, and they were indistinguishable in appearance, size, growth, development, and behavior from their littermates.

We first examined the epithelial architecture of the mouse lung where the LMO7 protein was expressed prominently. Lung sections of 5-week-old mice showed no difference between the WT and *LMO7*$^{-/-}$ mice (Fig. 3a), whereas lung sections of 14-week-old mice showed irregular epithelial sheets in the terminal and respiratory bronchioles and alveolar ducts of the *LMO7*$^{-/-}$ mice (Fig. 3b). Electron micrographs of the *LMO7*$^{-/-}$ mouse lung clearly showed changes in the epithelial architecture that protruded from the submucosa (Fig. 3c). The protruding lesions showed a characteristic feature composed of 9–10 epithelial cells. Cells with many secretory granules were located at the top of the lesion whereas electron density-rich cells were located at both sides of the bottom. Importantly, the basal membrane of the epithelial cells retained contacts with the basement membrane, resulting in elongation and invagination of the basement membrane toward the epithelial cells.

To further investigate whether or not these structural changes were associated with changes in apical junctions and epithelial polarity, we carried out immunostaining analyses for junctional components and apical surface marker proteins (Fig. 4). The signals for E-cadherin and catenins (Fig. 4a–d), as well as nectins and afadin (data not shown), were localized at the AJ although the positions of AJ were slightly deviated. The signals for ezrin were located at the apical membrane (Fig. 4e,f). The signals for filamentous actin and α-actinin were located at the cortical surface of the cells (Fig. 4g–j). These findings indicate that the cell–cell adhesions and apical–basal polarity of the epithelial cells did not change in the absence of LMO7.

Development of lung adenocarcinomas in mice lacking LMO7. Previous studies have proposed the possible involvement of LMO7 in hereditary human mammalian cancer,[27] the cell properties of pancreatic, colon, and breast cancers,[23–25] and TGF-β-induced migration of AH130 cells.[20] Therefore, the disorganization of lung epithelial architecture found in the *LMO7*$^{-/-}$ mice at younger ages (14–16 weeks) prompted us to investigate the occurrence of lung cancer.

In spite of the lung lesions, *LMO7*$^{-/-}$ mice survived for long periods comparable with WT mice. To investigate whether the epithelial architecture was further disorganized, we examined mice at over 90 weeks of age, which is almost identical to the natural life span of mice. Notably, lung cancer was observed in the *LMO7*$^{-/-}$ mice in the hybrid genetic background when compared with the WT mice (Table 2; Supporting Fig. S1a). In the WT mice, none of 19 mice developed lung cancer except one that was further identified as metastatic sarcoma. In contrast, 22% of the *LMO7*$^{-/-}$ mice and 13% of the *LMO7*$^{+/-}$ mice developed lung cancer. Furthermore, all of the tumor samples were diagnosed as adenocarcinoma (Fig. 5e,f), except for one adenoma (Fig. 5a,b) and one adenoma in hyperplasia (Fig. 5c,d) observed in the *LMO7*$^{-/-}$ mice (Supporting Table S1). The differences in incidence were statistically significant among the genotypes for LMO7 ($P < 0.05$). To examine whether or not LMO7 was inactivated in the lung tumors developed in the *LMO7*$^{+/-}$ mice, we analyzed LMO7 expression by immunostaining with two different antibodies (Fig. 5g,h; Supporting Fig. S1). The immunofluorescent signals for LMO7 were robust in bronchiolar epithelia and alveoli of the normal part but significantly reduced in the tumor part of the same preparation, suggesting that LMO7 function could be impaired. At present, however, we have no information on DNA sequences to detect loss of heterozygosity or critical mutations of *LMO7*. We next examined whether the predisposition to spontaneous lung cancer was observed in a different genetic background. We backcrossed the F_1 hybrid mice to C57BL6 mice for four generations, yet the mice lacking LMO7 still displayed a tendency to develop adenocarcinoma (Table 2). The mice on the C57BL/6 J background tended to develop less lung tumors than those on the mixed background probably because C57BL/6 J genetic traits suppress the occurrence of lung cancer. We found that the incidence of lung cancer development was not different between male and female mice, suggesting that estrogen exposure is unlikely to be a risk factor for lung carcinogenesis (Supporting Table S1). Thus, the susceptibility to lung cancer is fundamentally associated with the status of LMO7 deficiency.

To further characterize the cancer cells, the lesions of the *LMO7*$^{-/-}$ lung sections were stained by periodic acid–Schiff reaction and Alcian blue stain, and further analyzed by immunostaining with antibodies against Ki-67, cytokeratin, and vimentin (Supporting Fig. S2). These findings were consistent with the properties of proliferating adenocarcinoma, supporting

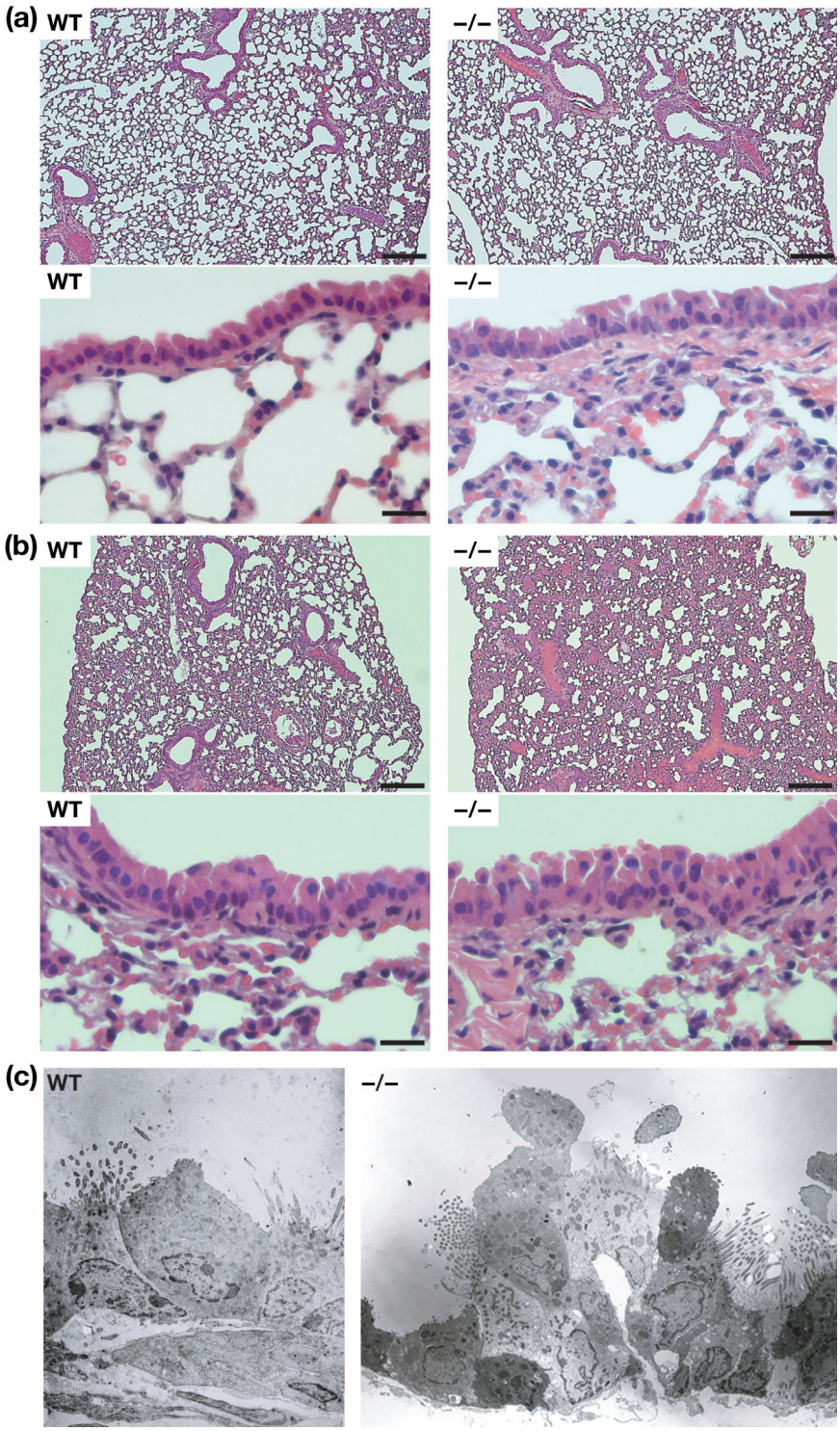

Fig. 3. Morphological changes in the lung of young LIM-domain only (*LMO*) *7*$^{-/-}$ mice. (a) Hematoxylin–eosin staining of lung sections from 5-week-old wild-type (WT) and *LMO7*$^{-/-}$ mice. Scale bar = 200 μm (upper panels), scale bar = 20 μm (lower panels). (b) Hematoxylin–eosin staining of lung sections from 14-week-old WT and *LMO7*$^{-/-}$ mice. Scale bar = 200 μm (upper panels), scale bar = 20 μm (lower panels). These WT and knockout (*LMO7*$^{-/-}$) mice were littermates. (c) Electron microscopy of the lung from WT and *LMO7*$^{-/-}$ littermate mice at 20 weeks of age.

the validity of pathological diagnoses. Finally, we extracted the cancer cells and cultured them *ex vivo*. The tumor cell lines derived from the lung cancer in *LMO7*$^{-/-}$ mice were successfully established. They showed numerical chromosome abnormalities (aneuploidy) (Supporting Fig. S3a) and tumor formation *in vivo* when subcutaneously injected into nude mice (Supporting Fig. S3b,c). Taken together, LMO7 deficiency caused disorganization of epithelial cells in the lung, eventually leading to development of adenocarcinomas, in agreement with a role for LMO7 as a tumor suppressor.

Discussion

Here we have shown that LMO7 has the potential to act as a tumor suppressor during mouse lung carcinogenesis. LMO7 plays important roles at the apical membrane and apical junctions, especially in the terminal and respiratory bronchioles where human lung adenocarcinoma frequently occurs. LMO7 deficiency causes disorganization of lung epithelial cells at a younger age, promotes cancer progression, and eventually leads to adenocarcinomas at older ages (Fig. 6). The observation that

doi: 10.1111/j.1349-7006.2009.01091.x

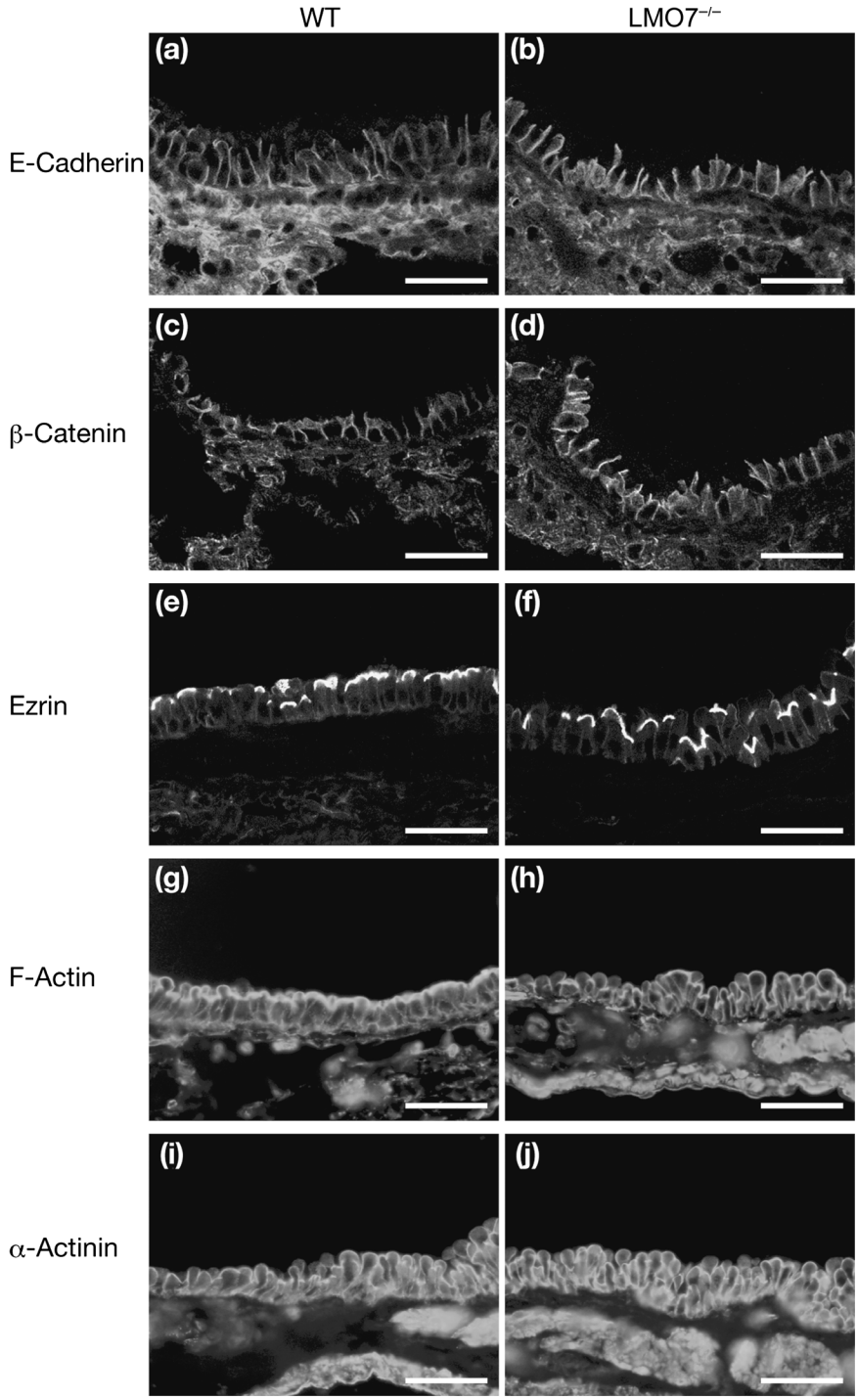

Fig. 4. Immunostaining of cell-adhesion components in the lung of young LIM-domain only (*LMO*) *7*$^{-/-}$ mice. Sections of terminal bronchioles obtained from wild-type (WT) and *LMO7*$^{-/-}$ littermate mice at 18 weeks of age are shown. (a,c,e,g,i) WT and (b,d,f,h,j) *LMO7*$^{-/-}$ lung sections were stained with antibodies for (a,b) E-cadherin, (c,d) β-catenin, (e,f) ezrin, (g,h) F-actin, and (i,j) α-actinin. Scale bar = 50 μm.

it took over 90 weeks for *LMO7*$^{-/-}$ mice to develop lung cancer and that the cumulative incidence of lung cancer was 22% in *LMO7*$^{-/-}$ mice suggests that secondary genetic events are required in this naturally occurring cancer model. Multiple mutations and epigenetic changes affecting key genes of cell proliferation and survival could explain the progression of lung cancer. It is of note that the incidence of lung cancer in *LMO7*$^{+/-}$ mice was approximately half of that in *LMO7*$^{-/-}$ mice, and that LMO7 was significantly expressed in normal epithelia but not in tumors in *LMO7*$^{+/-}$ mice, suggesting that LMO7 is correlated with conventional tumor suppressors that are compatible with the two-hit theory.[33] It remains to be clarified how and when these events are involved in developing spontaneous lung cancer.

The question of how the LMO7 protein functions as a tumor suppressor also remains unanswered. LMO7 has not been reported to inhibit cell-cycle progression or Ras-induced transformation. The large deletion (nearly 800 kb) covering the *Uchl3* and *LMO7* gene loci resulted in retinal and muscular degeneration and growth retardation.[32] Loss of full-length LMO7 might affect nuclear formation or cell mitosis in muscle fibers, although the phenotype could be attributed to loss of additional genes. In *LMO7*-knockdown cells in culture, the

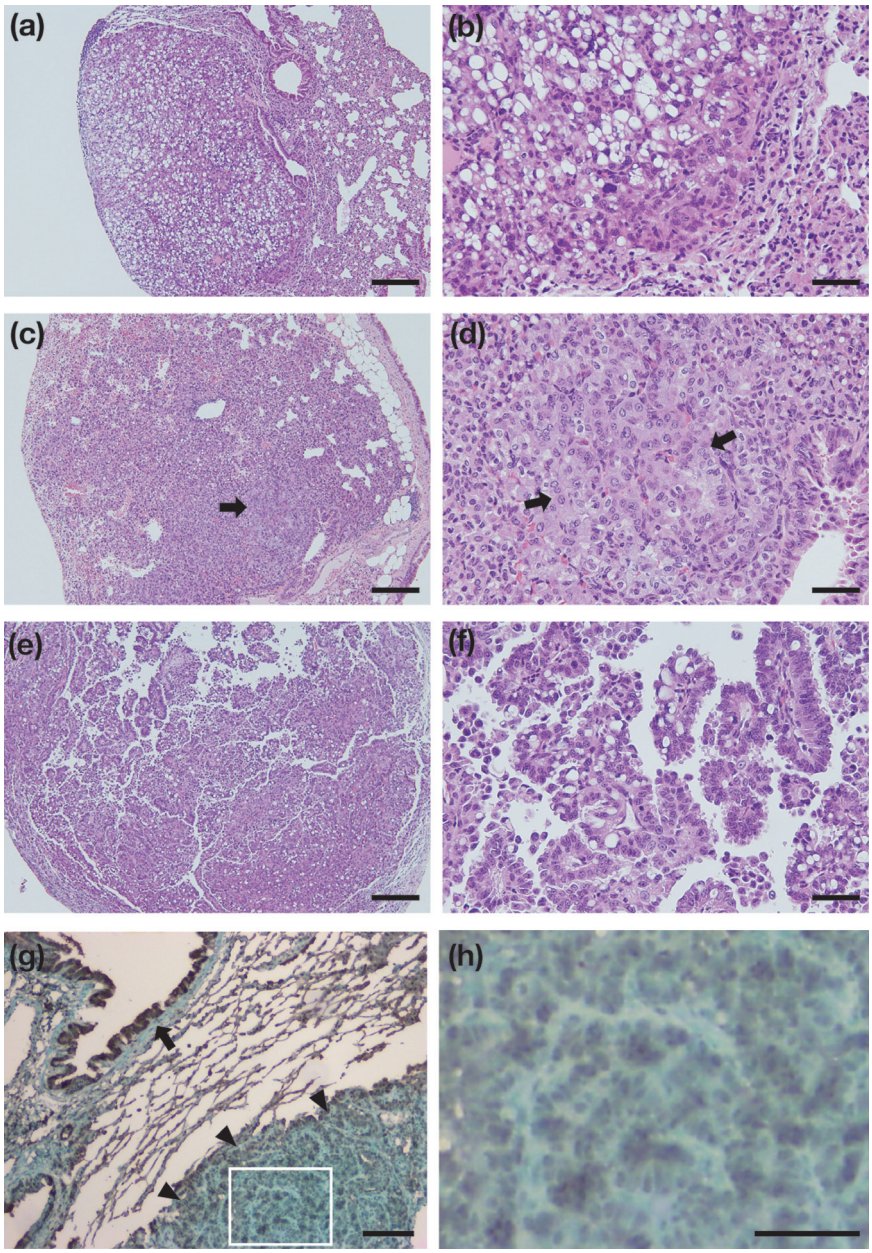

Fig. 5. Macroscopic and histological appearances of lung tumors obtained from LIM-domain only (*LMO*) *7*$^{-/-}$ mice and immunostaining of LMO7 in those obtained from *LMO7*$^{+/-}$ mice. Typical examples of (a,b) adenoma, (c,d) adenoma in hyperplasia, and (e,f) adenocarcinoma. Part of the adenoma is indicated by arrows in hyperplasia. (a,c,e) Scale bar = 200 μm, (b,d,f) scale bar = 50 μm. (g,h) Lung tumors in *LMO7*$^{+/-}$ mice were stained with the anti-LMO7 antibody #863. An arrow indicates bronchiolar epithelia displaying robust immunofluorescence signals for LMO7 and arrowheads indicate the boundary of the tumor. Tumor part indicated by an inset (g) is shown in a larger panel (h). (g) Scale bar = 100 μm, (h) scale bar = 50 μm.

expression of over 4000 genes, including *emerin*, has reportedly been changed.[26] Because emerin is a nuclear membrane protein and directly binds LMO7, LMO7 might function as a transcriptional regulator and might have antiproliferative effects, depending on the cellular context.

A close functional relationship must exist between loss of the PDZ domain of LMO7 and the disorganization of epithelial architecture observed in *LMO7*$^{-/-}$ mice. LMO7 could associate at least with α-actinin through the PDZ domain,[16] which specifically binds the C-terminal motifs of membrane-associated proteins, allowing the formation of a multiprotein complex. LMO7 can bind directly to the actin cytoskeleton through the N-terminal CH domain in LMO7 or indirectly by interaction with α-actinin.[16] Accordingly, epithelial cells lacking LMO7 cannot spread as a smooth epithelial sheet and tend to round, although they maintain their adhesions at the apical junctions. LMO7 may not be critically involved in the assembly of apical junction proteins, the exact mechanism of which remains unknown. Furthermore, they maintained the stable focal adhesions at the basal side that impair cell detachment. Lack of LMO7 thus appears to give them a protruding phenotype characteristically associated with invagination of the basement membrane, suggesting a possible role of LMO7 in modulating surface tensions between the apical and basal planes of the epithelia in the presence of intact adhesive complexes. Obviously, no other protein could replace the functions of LMO7 in the respiratory bronchioles in *LMO7*$^{-/-}$ mice. Although the molecular link between the loss of LMO7 and carcinogenesis is still missing, the structural and functional disorganization of the actin cytoskeleton is likely to underlie lung carcinogenesis.

Because LMO7 is exclusively located to the apical surface and junctions of epithelial cells, LMO7 may have a role in maintaining surface integrity, thereby protecting cells from invasion of microbes or extracellular irritants from the outer space of the body. Previously, we reported that an LMO7 splice variant, p100 #16/LMO7 lacking the C-terminal half of LMO7, was induced

doi: 10.1111/j.1349-7006.2009.01091.x

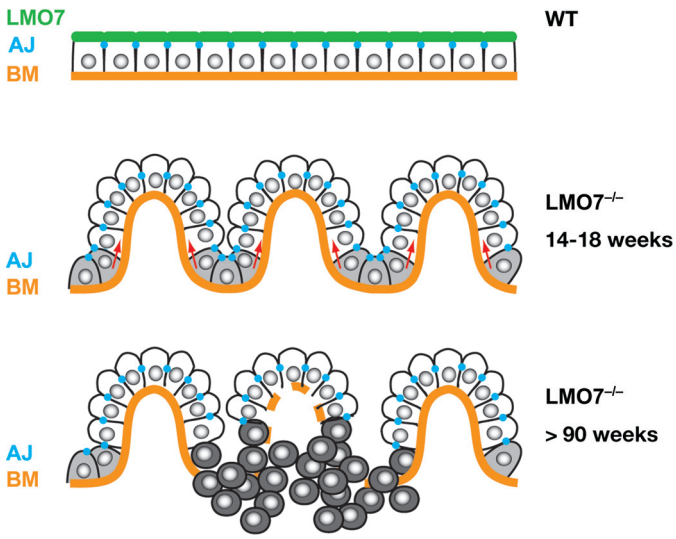

Fig. 6. Schematic model showing the potential role of LIM-domain only (LMO) 7 deficiency in lung cancer formation. Normally, LMO7 is localized to the apical membrane domain of the bronchiolar epithelial cells and modulates spreading of the epithelial sheets by balancing tensions between apical and basal cell planes. Loss of LMO7 promotes protrusions at the apical side and invagination of the basement membrane (BM), with the retention of cell–cell adhesion. It is also conceivable that the protruding bronchiolar epithelial lesions may reflect the abnormal outgrowth of cells lacking LMO7 at the basal ends of the protruding segments. The cells that are rich in electron density (indicated by gray tone) can continue to grow after the maturation of mice and then provide mechanical force to displace other cells laterally because of the limited space of bronchiolar airways. Disruption of epithelial integrity and additional cancer-promoting events would lead to cancer formation in some parts of *LMO7*$^{-/-}$ mice. AJ, adherens junction; WT, wild type.

in Yoshida hepatoma AH130W1 cells by TGF-β treatment.[20] TGF-β has been implicated in EMT by inducing expression of mesenchymal genes, as well as by downregulating the expression of E-cadherin. We presume that p100 #16/LMO7 might function as an activator of cell motility by inhibiting LMO7 function as MDCK cells expressing p100 #16/LMO7 showed a transformed cell shape and cytoplasmic and nuclear localization of LMO7 (Itoh Y, 2008, unpublished data). Thus, TGF-β could be implicated in cancer progression by inhibiting LMO7 function. The LMO7 proteins highly expressed in pancreatic, colorectal, and breast cancer[23–25] may play roles in promoting carcinogenesis although it remains unclear whether these proteins are mutated oncoproteins or variant forms of LMO7. Inhibition of full-length LMO7 function thus might be an underlying mechanism for the TGF-β-mediated progression of cancer of epithelial origin.

Deficiency of LMO7 is not implicated in mammary carcinogenesis in mice, as proposed in humans.[27–29] Although this discrepancy remains unsolved, it may not be attributed to the difference in tissue-specific expression of LMO7 because its expression profiles are almost the same between mice and humans. Actually, our preliminary studies using immunostaining have shown that reduced LMO7 expression is observed in some cases of human lung adenocarcinoma and appears to correlate with the malignant transformation of cancer cells (Nakamura H, 2008, unpublished data). Therefore, immunological detection of LMO7 proteins and reverse transcription-PCR assays detecting alternative splicing of p100 #16/LMO7 could be useful tools for evaluating the properties of human lung cancer, stages of carcinogenesis, and metastatic potential. Further studies on LMO7-deficient mice would provide us with new insights into spontaneous lung carcinogenesis.

Acknowledgments

This work was supported by Grants-in-Aid for Cancer Research from the Ministry of Education, Culture, Sports, Science, and Technology, Japan.

References

1 Miyoshi J, Takai Y. Structural and functional associations of apical junctions with cytoskelton. *Biochim Biophys Acta* 2008; **1778**: 670–91.
2 Gumbiner BM. Regulation of cadherin-mediated adhesion in morphogenesis. *Nature Rev Mol Cell Biol* 2005; **6**: 622–34.
3 Perez-Moreno M, Fuchs E. Catenins: keeping cells from getting their signals crossed. *Dev Cell* 2006; **11**: 601–12.
4 Takai Y, Miyoshi J, Ikeda W, Ogida H. Nectins and nectin-like molecules: roles in contact inhibition of cell movement and proliferation. *Nature Rev Mol Cell Biol* 2008; **9**: 603–15.
5 Vleminckx K, Vakaet L Jr, Mareel M, Fiers W, van Roy F. Genetic manipulation of E-cadherin expression by epithelial tumor cells reveals an invasion suppressor role. *Cell* 1991; **66**: 107–19.
6 Takeichi M. Cadherins in cancer: implication for invasion and metastasis. *Curr Opin Cell Biol* 1993; **5**: 803–11.
7 Perl AK, Wilgenbus P, Dahl U, Semb H, Christofori G. A causal role for E-cadherin in the transition from adenoma to carcinoma. *Nature* 1998; **392**: 190–3.
8 Hirohashi S. Inactivation of the E-cadherin-mediated cell adhesion system in human cancers. *Am J Pathol* 1999; **153**: 333–9.
9 Christofori G. New signals from the invasive front. *Nature* 2006; **441**: 444–50.
10 Harris BZ, Lim WA. Mechanism and role of PDZ domains in signaling complex assembly. *J Cell Sci* 2001; **114**: 3219–31.
11 Kadrmas JL, Beckerle MC. The LIM domain: from the cytoskeleton to the nucleus. *Nat Rev Mol Cell Bio* 2004; **5**: 920–31.
12 Xia H, Winokur ST, Kuo WL, Altherr MR, Bredt DS. Actinin-associated LIM protein: identification of a domain interaction between PDZ and spectrin-like repeat motif. *J Cell Biol* 1997; **139**: 507–15.
13 Zhou Q, Ruiz-Lozano P, Martone ME, Chen J. Cypher, a striated muscle-restricted PDA and LIM domain-containing protein, binds to alpha-actinin-2 and protein kinase C. *J Biol Chem* 1999; **274**: 19 807–13.
14 Bauer K, Kratzer M, Otte M *et al*. Human CLP36, a PDZ-domain and LIM-domain protein, binds to α-actinin-1 and associates with actin filaments and stress fibers in activated platelets and endothelial cells. *Blood* 2000; **96**: 4236–45.
15 Nakagawa K, Kuroda S. ENH, containing PDZ and LIM domains, heart/skeletal muscle-specific protein, associates with cytoskeletal proteins through the PDZ domain. *Biochem Biophys Res Commun* 2000; **272**: 505–12.
16 Ooshio T, Irie K, Morimoto K, Fukuhara A, Imai T, Takai Y. Involvement of LMO7 in the association of two cell–cell adhesion molecules, nectin and E-cadherin, through Afadin and α-actinin in epithelial cells. *J Biol Chem* 2004; **279**: 31 365–73.
17 Torrado M, Senatorov VV, Trivedi R, Fariss RN, Tomarev SI. Pdlim2, a novel PDZ-LIM domain protein, interacts with α-actinins and filamin A. *Invest Ophthalmol Vis Sci* 2004; **45**: 3955–63.
18 Vallenius T, Luukko K, Makela TP. CLP-36 PDZ-LIM protein associates with nonmuscle alpha-actinin-1 and alpha-actinin-4. *J Biol Chem* 2000; **275**: 11 100–5.
19 Vallenius T, Scharm B, Vesikansa A, Luukko K, Schafer R, Makela TP. The PDZ-LIM protein RIL modulates actin stress fiber turnover and enhances the association of α-actinin with F-actin. *Exp Cell Res* 2004; **293**: 117–28.
20 Nakamura H, Mukai M, Komatsu K *et al*. Transforming growth factor-b1 induces LMO7 while enhancing the invasiveness of rat ascites hepatoma cells. *Cancer Lett* 2005; **220**: 95–9.
21 Akedo H, Shinkai K, Mukai M *et al*. Interaction of rat ascites hepatoma cells with cultured mesothelial cell layers: a model for tumor invasion. *Cancer Res* 1986; **46**: 2416–22.
22 Mukai M, Shinkai K, Komatsu K, Akedo H. Potentiation of invasive capacity of rat ascites hepatoma cells by transforming growth factor-beta. *Jpn J Cancer Res* 1989; **80**: 107–10.
23 Kang S, Xu H, Duan X *et al*. *PCD1*, a novel gene containing PDZ and LIM domains, is overexpressed in several human cancers. *Cancer Res* 2000; **60**: 5296–302.
24 Furuya M, Tsuji N, Endoh T *et al*. A novel gene containing PDZ and LIM domains, PCD1, is overexpressed in human colorectal cancer. *Anticancer Res* 2002; **22**: 4183–6.
25 Sasaki M, Tsuji N, Furuya M *et al*. PCD1, a novel gene containing PDZ and LIM domains, is overexpressed in human breast cancer and linked to lymph node metastasis. *Anticancer Res* 2003; **23**: 2717–21.
26 Holaska JM, Rais-Bahrami S, Wilson KL. Lmo7 is an emerin-binding

protein that regulates the transcription of emerin and many other muscle-relevant genes. *Human Mol Genet* 2006; **15**: 3459–72.
27 Kainu T, Juo SH, Desper R *et al*. Somatic deletions in hereditary breast cancers implicate 13q21 as a putative novel breast cancer susceptibility locus. *Proc Natl Acad Sci USA* 2000; **97**: 9603–8.
28 Rozenblum E, Vahteristo P, Sandberg T *et al*. A genomic map of a 6-Mb region at 13q21-q22 implicated in cancer development: identification and characterization of candidate genes. *Human Genet* 2002; **110**: 111–21.
29 Thompson D, Szabo CI, Mangion J *et al*. Evaluation of linkage of breast cancer to the putative BRCA3 locus on chromosome 13q21 in 128 multiple case families from the Breast Cancer Linkage Consortium. *Proc Natl Acad Sci USA* 2002; **99**: 827–31.
30 Tanaka M, Miyoshi J, Ishizaki H *et al*. Role of Rab3 GDP/GTP exchange protein in synaptic vesicle trafficking at the mouse neuromuscular junction. *Mol Biol Cell* 2001; **12**: 1421–30.
31 Putilina T, Jaworski C, Gentleman S, Mcdonald B, Kadiri M, Wong P. Analysis of a human cDNA containing a tissue-specific alternatively spliced LIM domain. *Biochem Biophys Res Commun* 1998; **252**: 433–9.
32 Semenova E, Wang X, Jablonski MM, Levorse J, Tilghman SM. An engineered 800 kilobase deletion of Uchl3 and Lmo7 on mouse chromosome 14 causes defects in viability, postnatal growth and degeneration of muscle and retina. *Human Mol Genet* 2003; **12**: 1301–12.
33 Knudson AG Jr. Mutation and cancer: statistical study of retinoblastoma. *Proc Natl Acad Sci USA* 1971; **68**: 820–3.

Supporting Information

Additional Supporting Information may be found in the online version of this article:

Fig. S1. Characterization of lung tumors. (a) Macroscopic appearances of adenocarcinoma are shown. Lung tumors in LIM-domain only (*LMO*) $7^{+/-}$ and *LMO7*$^{-/-}$ mice were stained with the anti-LMO7 antibodies (b,c) #863, (d–f) #3528, and (g–i) NO2. LMO7 expression levels of tumor part obtained from (d,e,g,h) *LMO7*$^{+/-}$ mice were almost comparable to those of tumors obtained from (b,c,f,i) *LMO7*$^{-/-}$ mice. (b,d,g) Scale bar = 100 μm, (c,e,f,h,i) scale bar = 50 μm.

Fig. S2. Characterization of lung tumors obtained from LIM-domain only (*LMO*) $7^{-/-}$ mice. (a,b) Hematoxylin–eosin staining, (c,d) periodic acid–Schiff reaction, (e,f) alcian blue staining, (g,h) anti-Ki-67 staining, (i,j) anti-keratin staining, and (k,l) anti-vimentin staining are shown. Scale bar = 200 μm.

Fig. S3. *Ex vivo* properties of lung cancer cells. (a) Chromosomal abnormalities of cultured LIM-domain only (*LMO*) $7^{-/-}$ lung cancer cells. Scale bar = 30 μm. Over 70 chromosomes were detected. (b) Lung cancer cells implanted under the skin in nude mice. (c) Hematoxylin–eosin staining of a tumor mass raised in nude mice. Scale bar = 300 μm.

Table S1. Histopathology of lung cancer in LIM-domain only (LMO) 7-deficient mice and incidence of lung cancer between male (M) and female (F) mice

doi: 10.1111/j.1349-7006.2009.01091.x